JACS
JOURNAL OF THE AMERICAN CHEMICAL SOCIETY
Article
pubs.acs.org/JACS

Combining Electron-Neutral Building Blocks with Intramolecular "Conformational Locks" Affords Stable, High-Mobility P- and N-Channel Polymer Semiconductors

Hui Huang,[†] Zhihua Chen,[‡,#] Rocio Ponce Ortiz,[†,⊥,#] Christopher Newman,[‡] Hakan Usta,[‡] Sylvia Lou,[†] Jangdae Youn,[†] Yong-Young Noh,[§] Kang-Jun Baeg,[∥] Lin X. Chen,[†] Antonio Facchetti,*[,†] and Tobin Marks*[,†]

[†]Department of Chemistry and the Materials Research Center, Northwestern University, Evanston Illinois 60208, United States
[‡]Polyera Corporation, 8045 Lamon Avenue, Skokie, Illinois 60077, United States
[§]Department of Chemical Engineering, Hanbat National University, Daejeon, 305-719 (Republic of Korea)
[∥]Convergence Components & Materials Laboratory, Electronics and Telecommunications Research Institute (ETRI), Daejeon 305-350, Republic of Korea
[⊥]Department of Physical Chemistry, University of Malaga, Malaga 29071, Spain

Supporting Information

ABSTRACT: Understanding the relationship between molecular/macromolecular architecture and organic thin film transistor (TFT) performance is essential for realizing next-generation high-performance organic electronics. In this regard, planar π-conjugated, electron-neutral (i.e., neither highly electron-rich nor highly electron-deficient) building blocks represent a major goal for polymeric semiconductors, however their realization presents synthetic challenges. Here we report that an easily accessible (minimal synthetic steps), electron-neutral thienyl-vinylene (**TVT**)-based building block having weak intramolecular S···O "conformational locks" affords a new class of stable, structurally planar, solution-processable, high-mobility, molecular, and macromolecular semiconductors. The attraction of merging the weak **TVT** electron richness with supramolecular planarization is evident in the DFT-computed electronic structures, favorable MO energetics, X-ray diffraction-derived molecular structures, experimental lattice coehesion metrics, and excellent TFT performance. **TVT**-based polymer TFTs exhibit stable carrier mobilities in air as high as 0.5 and 0.05 $cm^2/V{\cdot}s$ (n- and p-type, respectively). All-TVT polymer-based complementary inverter circuitry exhibiting high voltage gains (~50) and ring oscillator circuitry with high f_{osc}(~1.25 kHz) is readily fabricated from these materials by simple inkjet printing.

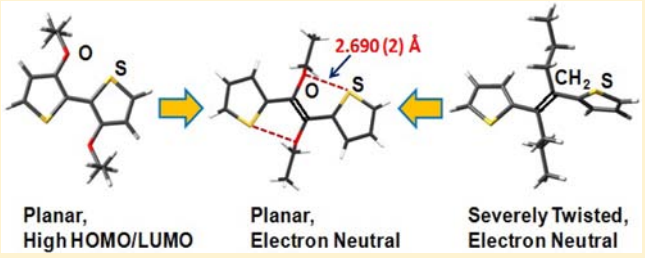

INTRODUCTION

Organic semiconductors have attracted intense academic and industrial research interest because of their potential for fabricating various opto-electronic devices, including active matrix organic light-emitting diodes (OLEDs),[1−4] organic photovoltaics (OPVs),[5−10] and organic thin film transistors (OTFTs).[11−17] OTFT devices are fundamental building blocks for organic integrated circuits that can be used as radio frequency identification cards, memories, sensors, and drivers for flexible displays. During the past several years, organic semiconductors have been shown to exhibit performance comparable to or exceeding that of amorphous silicon, the most common semiconductor used in display backplanes.[14] However, it is essential for realizing next-generation electronics that new semiconductors having higher mobility and greater current-carrying capacity than amorphous silicon be developed from rational principles. Furthermore, to fully capitalize on the attractions of organic electronic systems, it is critical to create organic semiconductors that can be processed by low-cost methodologies, such as spin coating and inkjet printing,[18] and which function in ambient environments without significant degradation.[19] Therefore, the rational synthesis of new organic semiconductors and understanding of the fundamental relationship between molecular/macromolecular architecture, lattice packing, and TFT performance are essential for next-generation low-cost, high-performance organic electronics. Furthermore, results to date indicate that such semiconductors must contain planar π-conjugated backbones to promote close solid-state $\pi-\pi$ stacking and efficient carrier transport via strong intermolecular orbital overlap.[20,21]

To achieve these critical advances,[22] rigorously planar, weakly electron-rich organic π-structures have been sought in the quest for solution-processable, air-stable, high-mobility polymer

Received: April 9, 2012
Published: June 8, 2012

semiconductors.[23−29] Promising building blocks include thiophenes and other heteraromatics, functionalized to enhance solubility and processability.[30,31] Depending on the electronic structure, p- or n-channel (hole or electron transporting, respectively) polymers can be created, with the best-performing typically being copolymers of electron-rich (for p-type) or electron-poor (for n-type) units, combined with weakly electron-rich cores. For the latter, the 2.2′-bithiophene core (**T2**; Chart 1) has afforded n- and p-channel copolymers with

Chart 1. Structures of 2.2′-Bithiophene (T2), 1,2-Di-(2-thienyl)-ethene (TVT) p-Channel Polymers PBTTT-R and P(TBTR-T2), and n-Channel Polymer P(NDI2OD-T2) (R = 2-octyldecyl)

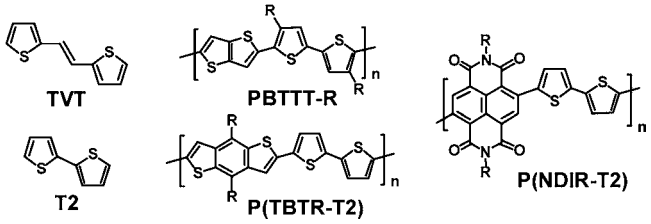

naphthalenediimide[32,33] or thienothiophene[34,35]/ benzodithiophene[36] fragments, respectively. Introducing other heteroatom groups can be used to promote planarity and enhance mobility,[37−43] however this typically requires complex and costly multiple-step syntheses. Weak covalent intramolecular interactions, as in O···S contacts between alkoxyl substituents and thiophenes, have been employed previously to promote macromolecular planarity.[44,45] However, much evidence shows that the strongly electron-donating alkoxy groups destabilize the π-system HOMOs[38] and significantly compromise the TFT performance and ambient stability.[46] Furthermore, combining alkoxy-thiophenes with electron-poor units favors low-bandgap, low-mobility ambipolar, rather than unipolar n-type, semiconductors.[47] Here we report a new design approach based on the **TVT** building block (Chart 1) functionalized with alkoxyl groups at the C=C linkage, which successfully addresses the above issues. We report that alkoxy-**TVT** derivatives, such as **M1** (Chart 2), offer four major attractions: (1) Two-step synthesis from commercially available monothiophenes having tunable alkoxy dimensions; (2) experimental and theoretical substantiation that alkoxy groups at the C=C linkage rather than at heteroaromatic positions minimally destabilize the HOMOs, thereby providing a versatile, electron-neutral building block for both p- and n-type semiconductors; (3) quantitiative X-ray diffraction and computational evidence that the O···S interaction functions as a "conformational lock," increasing planarity as well as carrier mobility; (4) synthetic flexibility allowing additional alkoxy group introduction to further enhance solubility and processability. Thus, **TVT**-based polymer TFTs exhibit carrier mobilities in air as high as 0.5 and 0.05 $cm^2/V{\cdot}s$ (n- and p-type, respectively) with good ambient stability. We also report that complementary all-**TVT** polymer inverters with high voltage gains (~50) and ring oscillator circuits with high f_{osc}(~1.25 kHz) can be readily fabricated from these materials by straightforward inkjet printing.

Chart 2. Structures of TVT-Based Monomers M1 and M2, Small Molecules SM1 and SM2, and Polymers P1−P4 (2OD = 2-octadecyl)

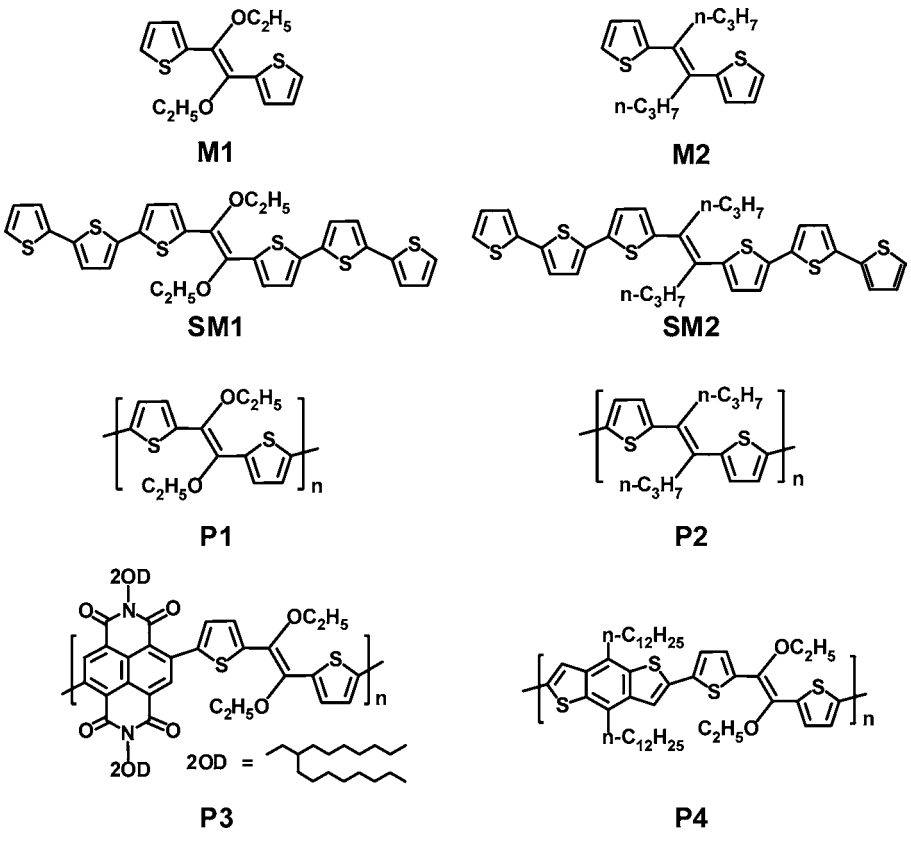

dx.doi.org/10.1021/ja303401s | J. Am. Chem. Soc. 2012, 134, 10966−10973

RESULTS AND DISCUSSION

Building Block and Polymer Synthesis and Characterization. The ethoxy-**TVT** building block **M1** was synthesized in two steps from thiophene (Scheme 1). Lithiation followed by addition of $Cr(CO)_6$ and $Et_3O{\cdot}BF_4$ affords a chromium carbene intermediate,[48] which is converted catalytically to an olefin **M1** in the presence of $Pd(PPh_3)_4$ with an overall yield >80%. For comparison, analogous **M2** with *n*-propyl substituents can be prepared through a McMurry reaction from an intermediate ketone,[49] also prepared from thiophene. Next, oligomers **SM1** and **SM2** were prepared via Stille coupling, starting from **M1** and **M2**, respectively (Scheme 2).

Scheme 1. Synthesis of Monomers M1 and M2

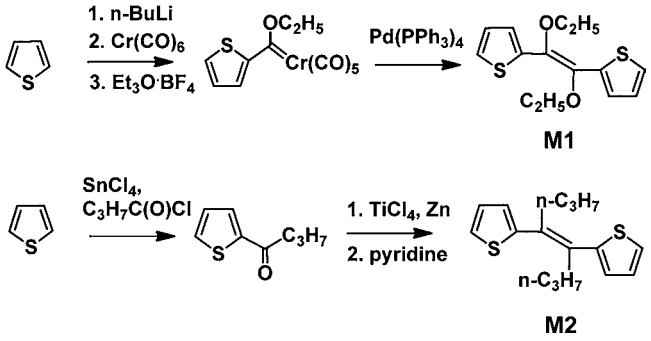

Homopolymers **P1** and **P2** were prepared via $FeCl_3$ oxidative polymerization of **M1** and **M2**, respectively. Both **P1** and **P2** have modest molecular weights as evaluated by gel permeation chromatography (GPC) at 150 °C (**P1**: M_n = 3.0 K, M_w = 3.4 K; **P2**: M_n = 2.7 K, M_w = 2.9 K). Copolymers **P3** and **P4** are readily accessed using various building blocks via Stille coupling (Scheme 2). **P3** is soluble in chloroform and chlorobenzene, and M_n = 18.6 K and M_w = 63.5 K. **P4** is also soluble in chlorinated solvents, and M_n = 12.4 K and M_w = 25.0 K.

Slow evaporation of an ethyl ether solution of **M1** afforded colorless crystals suitable for single crystal X-ray diffraction (XRD). The rigorous planarity of **M1** is evident in the crystal structure (Figure 1A), which contains cocrystallized, ∼97% of the low-energy sp,sp conformer and ∼3% of a higher-energy ap,ap conformer, similar to the situation in **TVT** crystals.[50,51] DFT computation shows that the sp,sp conformer is ∼1.15 kcal/mol lower in energy than the ap,ap conformer (Figures 1 and Supporting 1nformation). Importantly, the intramolecular O···S distance in **M1** is 2.690(2) Å, indicating a relatively strong O···S interaction.[45,52] **M1** crystallizes in a typical herringbone packing motif with a $\pi-\pi$ packing distance between neighboring molecules of 5.137 Å (Figure S1, Supporting 1nformation) and with no intermolecular O···S bonding. To further probe the importance of the O···S interaction in **TVT** planarity, the corresponding structure in which both thiophene rings are twisted from planarity, as found in **M2**, was computed by fixing the dihedral angles (see Figure S1, Supporting 1nformation). These results indicate that the planar structure is more stable by 8.3 kcal/mol. The effects of steric congestion on the conformation of **M2** can also be estimated by analyzing the energetic differences between the twisted, the more stable structure, and the less stable planar structure. As shown in Figure S1, Supporting 1nformation, the **M2** planar configuration, where the vinylene–thiophene dihedral angles are fixed

Scheme 2. Synthetic Routes to Small Molecule and Polymer Semiconductors[a]

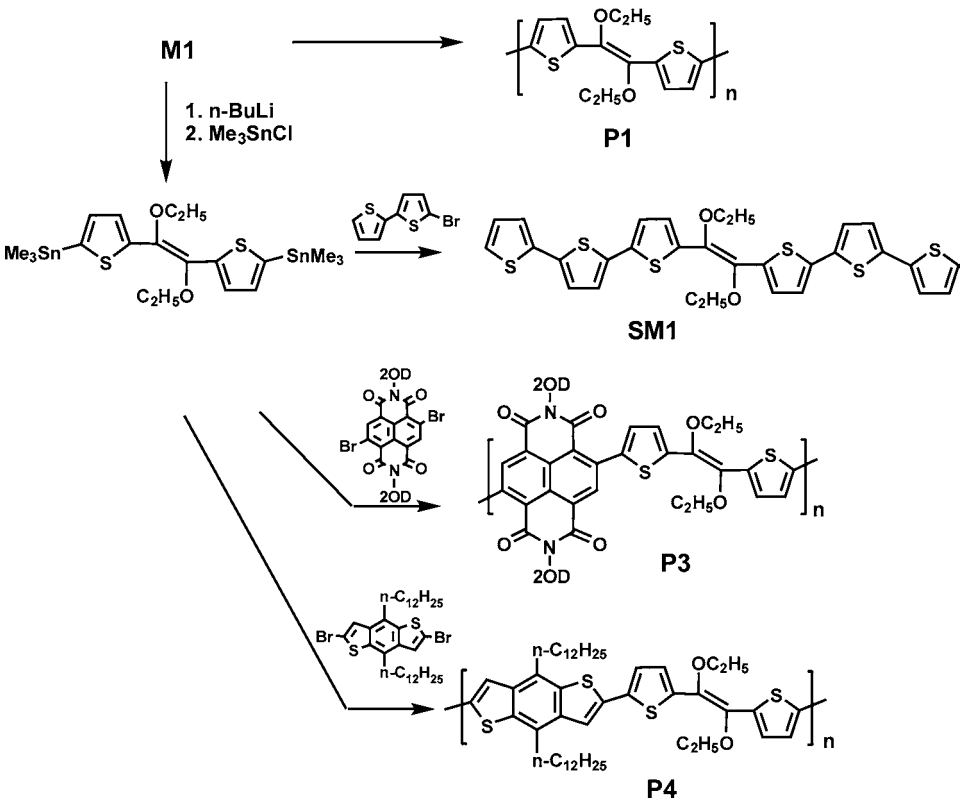

[a]2OD = 2-octyldecyl.

dx.doi.org/10.1021/ja303401s | J. Am. Chem. Soc. 2012, 134, 10966–10973

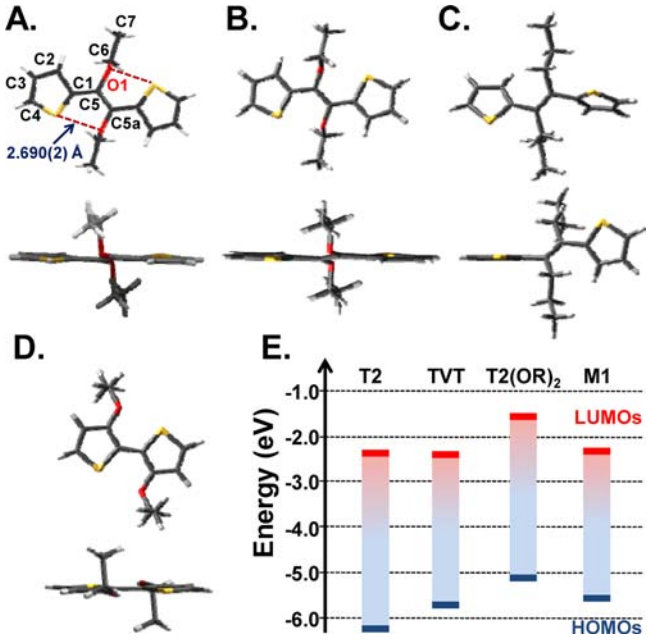

Figure 1. (A) Top and side views of the diffraction-derived molecular structure of **M1**. Selected bond lengths (Å) and angles (°) are C1−C5, 1.491(4); C5−C5a, 1.340(6); C5−O1, 1.411(3); C6−O1, 1.455(2); C1−C5−O1, 122.3(3);C1−C5−C5a, 122.1(4); O1−C5−C5a, 115.5(3). (B−D) Top and side views of the DFT//B3LYP/6-31G**-derived molecular structures of **M1**, **M2**, and **T2(OR)$_2$** (R = OC_2H_5), respectively. (E) Experimental HOMO/LUMO energies for the indicated systems.

at 180°, is less stable than the twisted one by 6.7 kcal/mol. This energetic difference is non-negligible, indicating significant steric repulsions between the CH_2 group and the S atom in **M2**. However, this value is smaller than the energetic difference found between **M1** planar and twisted configurations (8.3 kcal/mol) and points to the importance of the O···S conformational lock in **M1**.

The HOMO and LUMO energies of **M1** and **M2** obtained from cyclic voltammetry (CV) and optical spectroscopy are −5.6/−2.3 eV and −5.8/−2.2 eV, respectively (Table 1; Figure 1E and Figures S2 and S3, Supporting 1nformation). The smaller **M1** bandgap argues for greater π-system delocalization than in **M2**, which is supported by the DFT computations (Figure S4, Supporting 1nformation). Note that the HOMO and LUMO energies of **TVT** lie at −5.7/−2.4 eV,[53,54] respectively, only slightly different from those of **M1** (Figure 1E) and arguing that **M1** can serve as a electron-neutral building block for both n- and p-type π-semiconductors. In contrast to electron-neutral **T2**, the corresponding planar 3,3′-dialkoxy-2,2′-dithiophene **T2(OR)$_2$** (Figure 1D) with alkoxy-substituted thienyl rings, has far higher-lying MOs by ∼1 eV (HOMO/LUMO = −6.2/−2.4 vs −5.2/−1.6 eV, respectively), portending very different TFT characteristics. From the DFT calculations, the HOMO/LUMO energies of electron-neutral **T2** and **TVT** and the corresponding **T2(OR)$_2$** and **M1** molecules are computed to lie at −5.4/−1.2 and −5.2/−1.6 eV vs −4.7/−0.7 and −5.1/−1.3 eV, respectively, consistent with the aforementioned experimental data (Figure 1E and Figure S4, Supporting 1nformation). Not surprisingly, oligomer **SM1** (−5.4/−3.5 eV) has a smaller bandgap than **SM2** (−5.4/−3.1 eV), and this pattern extends to homopolymers **P1** and **P2**

Table 1. Thermal, Optical Absorption/Emission, Electrochemical, Field-Effect Mobility ($\mu_{e/h}$)[a], and Current I_{on}/I_{off} Ratio Data for Compounds M1-SM2 and P1−P4

Cmpd	Structure	mp [T_{DSC}[b]] (°C)	$E^{ox-1/2}$ [$E^{red-1/2}$] (V)	E_{LUMO} (eV)	E_{HOMO} (eV)	$\lambda_{abs}^{solution}$ (eV)	$\lambda_{abs}^{thin-film}$ (E_g(eV))	$\mu_{e/h}$ ($cm^2/V\cdot s$)	I_{on}/I_{off}
M1		158-159	+1.2	-2.3	-5.6	3.2	3.3	-	-
M2		oil	+1.4	-2.2	-5.8	3.6	3.6	-	-
SM1	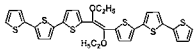	220-221 [218/173]	+1.0	-3.5	-5.4	2.4	1.9	3×10^{-3}	10^4
SM2	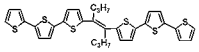	62-63	+1.0	-3.1	-5.4	2.5	2.3	inactive	-
P1	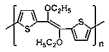	-	+0.8	-3.3	-5.2	2.0	1.9	3×10^{-6}	10^2-10^3
P2	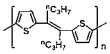	-	+1.1	-3.3	-5.5	2.4	2.2	inactive	-
P3	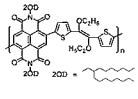	[220/200]	[-0.4]	-4.0	-5.4	1.5	1.4	0.2 0.5[c]	10^3 10^5
P4	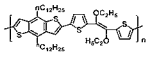	-	+0.7	-3.2	-5.1	2.2	1.9	0.02 0.05[c]	10^4 10^4

[a]Bottom-gate/top-contact structure if not stated otherwise. [c]Heating/cooling cycle. [c]Top-gate/bottom-contact structure.

dx.doi.org/10.1021/ja303401s | J. Am. Chem. Soc. 2012, 134, 10966−10973

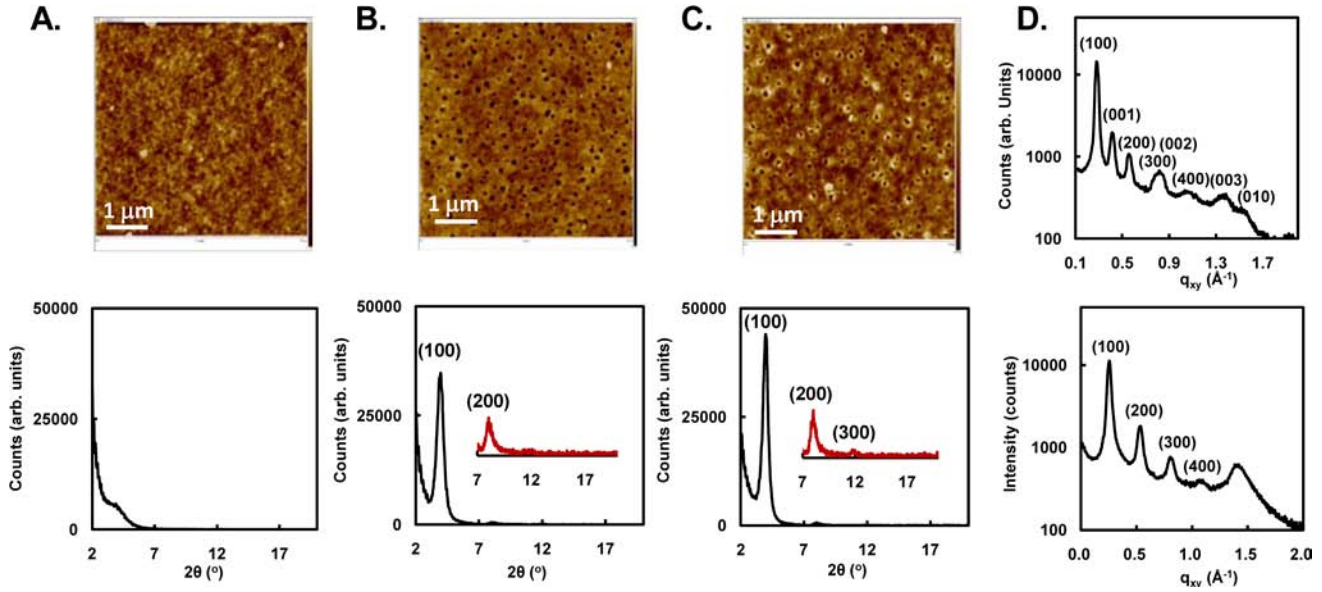

Figure 2. (A) Tapping mode AFM images (5 × 5 μm) and out-of-plane XRD scans of spin-coated **P3** thin films without annealing: (B) after annealing at 200 °C; (C) after annealing at 240 °C; and (D) in-plane (top) and out-of-plane (bottom) grazing incidence X-ray scattering of spin-coated **P3** thin films after annealing at 240 °C.

(Table 1). The LUMO and HOMO energies of copolymers **P3** and **P4** are −4.0/−5.4 and −3.2/−5.1 eV, respectively, essentially identical to those of analogous polymers **P(NDI2OD-T2)** and **P(TBTR-T2)** (Chart 1; −3.9/−5.4 and −3.0/−5.2 eV),[32,33,36] indicating that **M1** electronic properties are similar to those of weak electron-rich 2,2′-bithiophene. Note also that such low-lying **P3** LUMO (−4.0 eV) and **P4** HOMO energies portend significant TFT ambient stability.[46]

For closely related molecular materials, melting points are informative indices of lattice cohesion. Note that the **M1** melting point, 158−159 °C, is significantly higher than that of 1,2-di-(2-thienyl)-ethene, 133−134 °C.[55] Introducing alkyl or alkoxyl substituents on conjugated backbones typically depresses the melting points,[56] as in *E*-1,2-bis(3-methoxy-2-thienyl)ethene (mp 121−123 °C),[57] which is substantially lower melting than that of the 1,2-di-(2-thienyl)-ethene parent structure. The high **M1** melting point is reasonably attributable to the aforementioned O···S supramolecular backbone rigidification/planarization. Note that, in contrast to **M1**, compound **M2** is an oil at room temperature, doubtless due to the twisted backbone and looser intermolecular $\pi-\pi$ stacking, while the melting point of oligomer **SM1** is 220−221 °C, significantly higher than that of oligomer **SM2**, 62−63 °C. The thermogravimmetric analysis (TGA) data indicate that both **P3** and **P4** are thermally stable up to 280 °C, with less than 1% weight loss (Figure S5, Supporting 1nformation). The thermal transitions of the present materials were further investigated by DSC (Table 1, Figure S6, Supporting 1nformation). Oligomer **SM2** and polymers **P1**, **P2**, and **P4** exhibit no detectable endotherms/exotherms in the heating/cooling cycles, while oligomer **SM1** exhibits a single endothermic transition at 218 °C, tentatively attributable to backbone melting and an exothermic recrystallization peak at 173 °C. Polymer **P3** exhibits a broad endotherm at 220 °C and an exotherm at 200 °C, arguing that microstructural order is enhanced by annealing.

Thin Film Microstructural Characterization. AFM and XRD images (Figure 2) indicate that, in contrast to **P4** (Figure S7, Supporting 1nformation), the **P3** film morphology and microstructure change on annealing. AFM images of **P3** suggest that the morphology varies in a way suggesting that defects develop due to inadequate wetting during film formation, thereby creating a nonoptimal interface with the substrate. However, out-of-plane XRD reveals that **P3** films become significantly more crystalline on annealing (Figure 2). A single family of Bragg reflections is observed without the obvious $\pi-\pi$ stacking distance; the observed *d*-spacing is ∼22.2 Å after 200 °C annealing and is reasonably assigned to *a*-axis (*h*00) lamellar spacing. This distance is consistent with structural models in which the polymer side chains are either interdigitated or closely packed and tilted out of the molecular plane, implicating a polymorph in which most molecules have an edge-on orientation with respect to the substrate and with the $\pi-\pi$ stacking axis parallel to the substrate plane, thus favoring in-plane source → drain charge transport.[58] The crystallinity of the solution-cast **P3** films depends on the annealing temperature, with a major evolution in long-range order (Figure 2) and increasing crystallinity on increasing the annealing temperature from 200 to 240 °C. A significant increase in the (100) reflection intensity and the appearance of higher order reflections up to (300) is observed, while the *d*-spacing remains unchanged, indicating far greater intragrain ordering. In-plane microstructure was also analyzed by grazing incidence synchrotron X-ray scattering to better understand $\pi-\pi$ stacking in the highly crystalline **P3** films (Figure 2d). The 240 °C annealed films exhibit a (010) feature consistent with a $\pi-\pi$ stacking distance (4.11 Å), slightly larger than in **P(NDI2OD-T2)** (3.93 Å).[59] The other features can be indexed as (00*l*) reflections based on a tentative orthorhombic cell with the *c* axis equal to the repeat unit (15.1 Å), consistent with the DFT results (15.6 Å). All other things being equal, this substantial domain ordering should favor charge transport.

Field-Effect Transistor Fabrication and Measurements. Bottom-gate/top-contact (BGTC) and top-gate/bottom-contact (TGBC) geometry TFTs were fabricated on HMDS-treated p^+-Si/SiO_2 and glass substrates, respectively.

dx.doi.org/10.1021/ja303401s | *J. Am. Chem. Soc.* 2012, 134, 10966−10973

Data are summarized in Table 1 and Figure 3. The hole mobilities of oligomer **SM1** and homopolymer **P1** are 3×10^{-3}

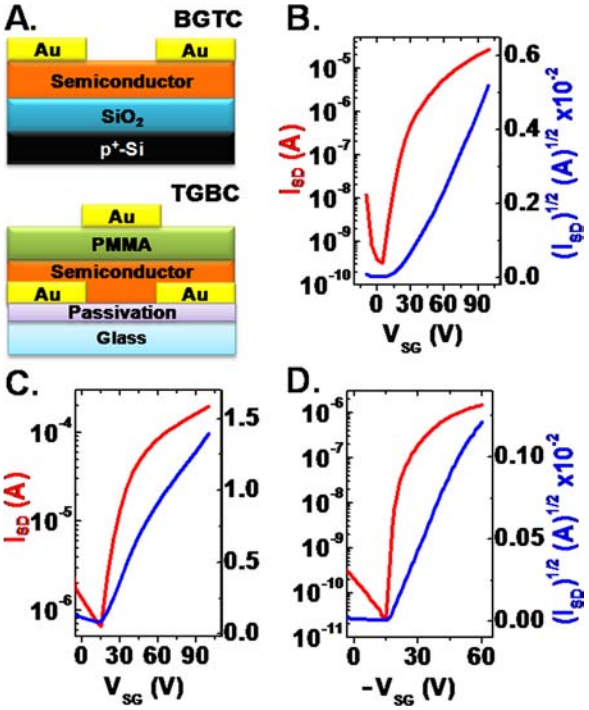

Figure 3. (A) Transistor architectures employed in this study. TFT transfer plots for polymers **P3** in (B) BGTC and (C) TGBC structures. (D) **P4** in a BGTC structure at $V_{SD} = -100$ V.

and 3×10^{-6} $cm^2/V{\cdot}s$, respectively, while **SM2** and homopolymer **P2** based on the extensively twisted **M2** building block are both TFT inactive. Films of **P3** exhibit n-type behavior, and the electron mobility without annealing is 2.3×10^{-3} $cm^2/V{\cdot}s$, consistent with the low crystallinity evident in Figure 2a. However, annealing at 200 °C increases the mobility to ~0.2 $cm^2/V{\cdot}s$, among the highest reported to date for an n-type polymer in a BGTC TFT architecture (Figure 3A),[60] while a TGBC device affords an increased electron mobility of ~0.5 $cm^2/V{\cdot}s$ in ambient (Figure 3B). Note that the high film crystallinity assayed by the XRD data closely parallels the TFT results. Note also that the electron mobility falls to $1.5 \times 10^{-3} cm^2/V{\cdot}s$ on annealing the films at 240 °C, although the crystallinity is slightly increased as judged by the XRD results. That increased crystallinity does not necessarily correlate with increased mobility is reasonable since transport across grain boundaries can significantly limit organic TFT performance.[35] All of the present TFTs exhibit significant ambient stability, in accord with the low-lying LUMOs. After eight months in laboratory air, the ambient mobility of the TFTs with TGBC structures falls from 0.11 to 0.05 $cm^2/V{\cdot}s$. The maximum hole mobility of copolymer **P4** in a TGBC device, 0.05 $cm^2/V{\cdot}s$, is achieved after thermal annealing in air at 130 °C for 1 h (Figure 3). The mobility of **P4** is moderate compared to other copolymers based on benzodithiophene building blocks.[61]

Organic Complementary Circuits. Complementary inverter and ring oscillator circuits were next fabricated from **P3** and **P4** by inkjet printing (Figure 4). For monolithic integration of the p- and n-channel OTFTs, the **P3** and **P4** solutions were sequentially printed onto photolithography patterned Au bottom-contact electrodes. The poly(methylmethacrylate)

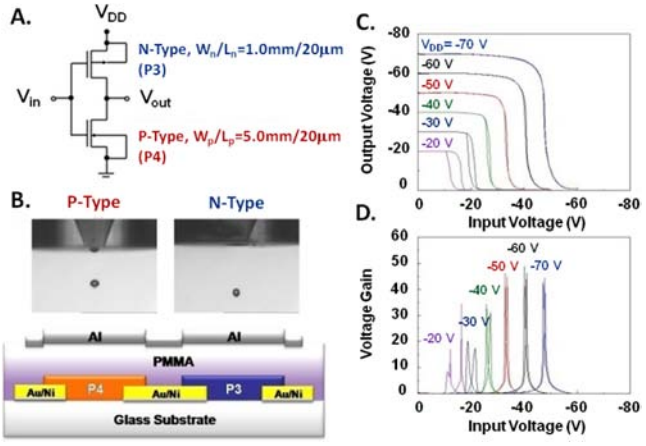

Figure 4. Complementary inverters fabricated from the **P3** (n-channel) + **P4** (p-channel) materials set. (A) Schematic electrical layout of the inverters. (B) Optical image of the inkjet-printed droplets and of the TFT structure used in the inverter. (C) Static switching characteristics of an inkjet-printed inverter with a PMMA gate dielectric. (D) Gain data for the inkjet-printed devices.

gate dielectric was spin-coated on top and via holes defined by selective removal of dielectric layer portions with inkjetted solvent. Figure 4 shows the voltage transfer characteristics of a complementary inverter fabricated with **P3** and **P4** (p and n-type, respectively) (W_p/L_p= 5.0 mm/20 μm, W_n/L_n =1.0 mm/20 μm) at various supply voltages (V_{DD}). Note that the static inverter characteristics exhibit negligible bias hysteresis and high voltage gains (~50) above $V_{DD} = -50$ V. The inverting point (V_{inv}) of the complementary inverter is reached when both the p- and n-channel transistors are operating in the saturation region[62] and is expressed by eq 1:

$$V_{inv} = \frac{V_{DD} + V_{Th}^{p} + V_{Th}^{n}\sqrt{\frac{\beta_n}{\beta_p}}}{1 + \sqrt{\frac{\beta_n}{\beta_p}}} \quad (1)$$

where the $\beta = (W/L)\mu_{FET}C_i$ is a design factor to adjust the p- and n-channel currents of transistors, and the superscripts p and n denote the semiconductor type. The V_{inv} of our device was slightly shifted in the negative direction, by ~ −15 V (at $V_{DD} = -70$ V) from the ideal switching position at 1/2 V_{DD}, and the W_p/L_p vs W_n/L_n ratio was modified to 5:1 for enhancing β_p compared to β_n. This was mainly attributed to the higher $\mu_{FET,e}$ (~10×) of the P3 (n-type) OFET than that of P4 (p-type) OFET, since the other parameters, such as V_{DD} and C_i, were equal to both p- and n-type OFETs. It is noted that the factor β must be carefully designed to optimize the performance of complementary circuits. The inverting voltage (V_{inv}) is slightly shifted in the negative direction with respect 1/2 V_{DD} due to the slight V_{Th} and mobility differences between the p- and n-type materials. For further integration of **P3**- and **P4**-based OTFTs, the dynamic switching characteristics in the present circuits were next evaluated using a complementary ring oscillator ($L_n = L_p$= 10 μm; $W_n = W_p$= 10 mm). A top view of inkjet-printed features of **P3** and **P4** and the completed polymer ring oscillator are shown in Figure S8, Supporting 1nformation. The oscillation frequencies (f_{osc}) of this circuit exhibit a strong dependence on V_{DD}, and the highest f_{osc} of ~1.25 kHz is obtained at $V_{DD} = 100$ V. Note that the device speed would be further increased by reducing gate to source

dx.doi.org/10.1021/ja303401s | J. Am. Chem. Soc. 2012, 134, 10966−10973

and drain electrode overlap capacitances,[63] and by using alternative gate dielectrics.[64]

CONCLUSIONS

These results demonstrate a versatile, electron-neutral, planar π-electron building block offering both "conformational locks" and appropriate HOMO/LUMO energetics to enforce π-system planarity, high carrier mobility, solution processability, and ambient stability for both p- and n-type organic semiconductors. **TVT**-based polymer TFTs exhibit carrier mobilities in air as high as 0.5 and 0.05 $cm^2/V{\cdot}s$ (n- and p-type, respectively). Using a n- and p-type variant of the same material permits fabrication of high-performance complementary inverters (voltage gains $\approx$ 50) and ring oscillators ($f_{osc} \approx$ 1.25 kHz) by simple inkjet printing. Furthermore, these results provide fundamental insight into the interrelationships between molecular/macromolecular architecture and organic TFT performance and durability.

ASSOCIATED CONTENT

Supporting Information

Monomer/polymer synthesis and characterization, ^1H and ^{13}C NMR spectra, XPS spectra, UV−vis spectra, DFT calculations, DSC and TGA traces, OTFT fabrication details, OTFT device data, and thin-film characterization (XRD and AFM) for different polymer deposition conditions. This material is available free of charge via the Internet at http://pubs.acs.org.

AUTHOR INFORMATION

Corresponding Author

a-facchetti@northwestern.edu; t-marks@northwestern.edu

Author Contributions

[#]These authors contributed equally.

Notes

The authors declare no competing financial interest.

ACKNOWLEDGMENTS

We thank AFOSR (FA9550-08-1-0331) and Polyera Corp. for support of this research at Northwestern University. We thank the NSF-MRSEC program through the Northwestern Materials Research Center (DMR-1121262) for support of characterization facilities. R.P.O. acknowledges funding from the European Community's Seventh Framework Programme through a Marie Curie International Outgoing Fellowship (grant agreement 234808). Use of the Advanced Photon Source was supported by the U. S. Department of Energy, Office of Science, Office of Basic Energy Sciences, under Contract No. DE-AC02-06CH11357.

REFERENCES

(1) Grimsdale, A. C.; Leok Chan, K.; Martin, R. E.; Jokisz, P. G.; Holmes, A. B. *Chem. Rev.* **2009**, *109*, 897−1091.

(2) Duan, L.; Qiao, J.; Sun, Y.; Qiu, Y. *Adv. Mater.* **2011**, *23*, 1137−1144.

(3) Cai, M.; Xiao, T.; Hellerich, E.; Chen, Y.; Shinar, R.; Shinar, J. *Adv. Mater.* **2011**, *23*, 3590−3596.

(4) Ahmed, E.; Earmme, T.; Jenekhe, S. A. *Adv. Funct. Mater.* **2011**, *21*, 3889−3899.

(5) Ko, S.; Verploegen, E.; Hong, S.; Mondal, R.; Hoke, E. T.; Toney, M. F.; McGehee, M. D.; Bao, Z. *J. Am. Chem. Soc.* **2011**, *133*, 16722−16725.

(6) Osaka, I.; Shimawaki, M.; Mori, H.; Doi, I.; Miyazaki, E.; Koganezawa, T.; Takimiya, K. *J. Am. Chem. Soc.* **2012**, *134*, 3498−3507.

(7) Zheng, Q.; Jung, B. J.; Sun, J.; Katz, H. E. *J. Am. Chem. Soc.* **2010**, *132*, 5394−5404.

(8) Son, H. J.; He, F.; Carsten, B.; Yu, L. *J. Mater. Chem.* **2011**, *21*, 18934−18945.

(9) Brabec, C. J.; Gowrisanker, S.; Halls, J. J. M.; Laird, D.; Jia, S.; Williams, S. P. *Adv. Mater.* **2010**, *22*, 3839−3856.

(10) Li, C.; Wonneberger, H. *Adv. Mater.* **2012**, *24*, 613−636.

(11) Oliva, M. M.; Casado, J.; Navarrete, J. T. L.; Patchkovskii, S.; Goodson, T., III; Harpham, M. R.; Seixas de Melo, J. S.; Amir, E.; Rozen, S. *J. Am. Chem. Soc.* **2011**, *132*, 6231−6242.

(12) Giri, G.; Verploegen, E.; Mannsfeld, S. C. B.; Atahan-Evrenk, S.; Kim, D. H.; Lee, S. Y.; Becerril, H. A.; Aspuru-Guzik, A.; Toney, M. F.; Bao, Z. *Nature* **2011**, *480*, 504−508.

(13) Lee, T.; Landis, C. A.; Dhar, B. M.; Jung, B. J.; Sun, J.; Sarjeant, A.; Lee, H.-J.; Katz, H. E. *J. Am. Chem. Soc.* **2009**, *131*, 1692−1705.

(14) Takimiya, K.; Shinamura, S.; Osaka, I.; Miyazaki, E. *Adv. Mater.* **2011**, *23*, 4347−4370.

(15) Santato, C.; Cicoira, F.; Martel, R. *Nat. Photonics* **2011**, *5*, 392−393.

(16) Jung, B. J.; Tremblay, N. J.; Yeh, M.-L.; Katz, H. E. *Chem. Mater.* **2011**, *23*, 568−582.

(17) Usta, H.; Facchetti, A.; Marks, T. J. *Acc. Chem. Res.* **2011**, *44*, 501−510.

(18) Katz, H. E. *Chem. Mater.* **2004**, *16*, 4748−4756.

(19) Bobbert, P. A.; Sharma, A.; Mathijssen, S. G. J.; Kemerink, M.; de Leeuw, D. M. *Adv. Mater.* **2012**, *24*, 1146−1158.

(20) Salleo, A.; Kline, R. J.; DeLongchamp, D. M.; Chabinyc, M. L. *Adv. Mater.* **2010**, *22*, 3812−3838.

(21) Sirringhaus, H.; Bird, M.; Zhao, N. *Adv. Mater.* **2010**, *22*, 3893−3898.

(22) Beaujuge, P. M.; Frechet, J. M. J. *J. Am. Chem. Soc.* **2011**, *133*, 20009−20029.

(23) Zhan, X.; Facchetti, A.; Barlow, S.; Marks, T. J.; Ratner, M. A.; Wasielewski, M. R.; Marder, S. R. *Adv. Mater.* **2011**, *23*, 268−284.

(24) Bronstein, H.; Chen, Z.; Ashraf, R. S.; Zhang, W.; Du, J.; Durrant, J. R.; Shakya Tuladhar, P.; Song, K.; Watkins, S. E.; Geerts, Y.; Wienk, M. M.; Janssen, R. A. J.; Anthopoulos, T.; Sirringhaus, H.; Heeney, M.; McCulloch, I. *J. Am. Chem. Soc.* **2011**, *133*, 3272−3275.

(25) Beaujuge, P. M.; Reynolds, J. R. *Chem. Rev.* **2010**, *110*, 268−320.

(26) McCulloch, I.; Heeney, M.; Chabinyc, M. L.; De Longchamp, D.; Kline, R. J.; Colle, M.; Duffy, W.; Fischer, D.; Gundlach, D.; Hamadani, B.; Hamilton, R.; Richter, L.; Salleo, A.; Shkunov, M.; Sparrowe, D.; Tierney, S.; Zhang, W. *Adv. Mater.* **2009**, *21*, 1091−1109.

(27) Allard, S.; Forster, M.; Souharce, B.; Thiem, H.; Scherf, U. *Angew. Chem., Int. Ed.* **2008**, *47*, 4070−4098.

(28) Newman, C. R.; Frisbie, C. D.; da Silva Filho, D. A.; Bredas, J.-L.; Ewbank, P. C.; Mann, K. R. *Chem. Mater.* **2004**, *16*, 4436−4451.

(29) Roncali, J. *Chem. Rev.* **1992**, *92*, 711−38.

(30) Facchetti, A. *Chem. Mater.* **2011**, *23*, 733−758.

(31) Marks, T. J. *MRS Bull.* **2010**, *35*, 1018−1027.

(32) Chen, Z.; Zheng, Y.; Yan, H.; Facchetti, A. *J. Am. Chem. Soc.* **2009**, *131*, 8−9.

(33) Yan, H.; Chen, Z.; Zheng, Y.; Newman, C.; Quinn, J. R.; Dotz, F.; Kastler, M.; Facchetti, A. *Nature* **2009**, *457*, 679−686.

(34) Li, Y. N.; Singh, S. P.; Sonar, P. *Adv. Mater.* **2010**, *22*, 4862−4866.

(35) (a) McCulloch, I.; Heeney, M.; Bailey, C.; Genevicius, K.; MacDonald, I.; Shkunov, M.; Sparrowe, D.; Tierney, S.; Wagner, R.; Zhang, W.; Chabinyc, M. L.; Kline, R. J.; McGehee, M. D.; Toney, M. F. *Nat. Mater.* **2006**, *5*, 328−333. (b) Rivnay, J.; Jimison, L. H.; Toney, M. F.; Noriega, R.; Marks, T. J.; Facchetti, A.; Salleo, A. *Nat. Mater.* **2009**, *8*, 952−958.

(36) Sista, P.; Hao, J.; Elkassih, S.; Sheina, E. E.; Biewer, M. C.; Janesko, B. G.; Stefan, M. C. *J. Polym. Sci., Part A: Polym. Chem.* **2011**, *49*, 4172−4179.

(37) Wu, W.; Liu, Y.; Zhu, D. *Chem. Soc. Rev.* **2010**, *39*, 1489−1502.
(38) Roncali, J. *Macromol. Rapid Commun.* **2007**, *28*, 1761−1775.
(39) Usta, H.; Lu, G.; Facchetti, A.; Marks, T. J. *J. Am. Chem. Soc.* **2006**, *128*, 9034−9035.
(40) Usta, H.; Risko, C.; Wang, Z.; Huang, H.; Deliomeroglu, M. K.; Zhukhovitskiy, A.; Facchetti, A.; Marks, T. J. *J. Am. Chem. Soc.* **2009**, *131*, 5586−5608.
(41) Fong, H. H.; Pozdin, V. A.; Amassian, A.; Malliaras, G. G.; Smilgies, D. M.; He, M. Q.; Gasper, S.; Zhang, F.; Sorensen, M. *J. Am. Chem. Soc.* **2008**, *130*, 13202−13203.
(42) He, M. Q.; Li, J. F.; Sorensen, M. L.; Zhang, F. X.; Hancock, R. R.; Fong, H. H.; Pozdin, V. A.; Smilgies, D. M.; Malliaras, G. G. *J. Am. Chem. Soc.* **2009**, *131*, 11930−11938.
(43) Guo, X.; Ortiz, R. P.; Zheng, Y.; Hu, Y.; Noh, Y.-Y.; Baeg, K.-J.; Facchetti, A.; Marks, T. J. *J. Am. Chem. Soc.* **2011**, *133*, 1405−1418.
(44) Roncali, J.; Blanchard, P.; Frere, P. *J. Mater. Chem.* **2005**, *15*, 1589−1610.
(45) Guo, X.; Kim, F. S.; Jenekhe, S. A.; Watson, M. D. *J. Am. Chem. Soc.* **2009**, *131*, 7206−7207.
(46) de Leeuw, D. M.; Simenon, M. M. J.; Brown, A. R.; Einerhand, R. E. F. *Synth. Met.* **1997**, *87*, 53−59.
(47) Kim, F. S.; Guo, X.; Watson, M. D.; Jenekhe, S. A. *Adv. Mater.* **2010**, *22*, 478−482.
(48) Terblans, Y. M.; Marita Roos, H.; Lotz, S. *J. Organomet. Chem.* **1998**, *566*, 133−142.
(49) Kosak, A. I.; Hartough, H. D. *Org. Synth.* **1948**, *28*, 1−2.
(50) Ruban, G.; Zobel, D. *Acta Crystallogr., Sect. B* **1975**, *B31*, 2632−2634.
(51) Blockhuys, F.; Vande Velde, C. M. L.; Maes, S. T.; Peten, C.; Geise, H. J.; Van Alsenoy, C.; Lenstra, A. T. H. *Acta Crystallogr., Sect. B* **2003**, *B59*, 770−778.
(52) Vangheluwe, M.; Verbiest, T.; Koeckelberghs, G. *Macromolecules* **2008**, *41*, 1041−1044.
(53) Roncali, J.; Thobie-Gautier, C.; Elandaloussi, E. H.; Frere, P. *J. Chem. Soc, Chem. Comm* **1994**, 2249−50.
(54) Garcia, M. H.; Florindo, P.; Piedade, M. F. M.; Duarte, M. T.; Robalo, M. P.; Goovaerts, E.; Wenseleers, W. *J. Organomet. Chem.* **2009**, *694*, 433−445.
(55) Starcevic, K.; Boykin, D. W.; Karminski-Zamola, G. *Heteroat. Chem.* **2003**, *14*, 218−222.
(56) Bao, Z. N.; Chen, Y. M.; Cai, R. B.; Yu, L. P. *Macromolecules* **1993**, *26*, 5281−5286.
(57) Blockhuys, F.; Hoefnagels, R.; Peten, C.; Van Alsenoy, C.; Geise, H. J. *J. Mol. Struct.* **1999**, *485−486*, 87−96.
(58) Zaumseil, J.; Sirringhaus, H. *Chem. Rev.* **2007**, *107*, 1296−1323.
(59) Rivnay, J.; Toney, M. F.; Zheng, Y.; Kauvar, I. V.; Chen, Z.; Wagner, V.; Facchetti, A.; Salleo, A. *Adv. Mater.* **2010**, *22*, 4359−4363.
(60) Sonar, P.; Singh, S. P.; Li, Y.; Soh, M. S.; Dodabalapur, A. *Adv. Mater.* **2010**, *22*, 5409−5413.
(61) Pan, H.; Wu, Y.; Li, Y.; Liu, P.; Ong, B. S.; Zhu, S.; Xu, G. *Adv. Funct. Mater.* **2007**, *17*, 3574.
(62) Rabaey, J.M.; Chandrakasan, A.; Nikolić, B. *Digital Integrated Circuits*, 2nd ed.; Prentice Hall: Upper Saddle River, NJ, 2003.
(63) Noh, Y.-Y.; Zhao, N.; Caironi, M.; Sirringhaus, H. *Nat. Nanotechnol.* **2007**, *2*, 784−789.
(64) (a) Ortiz, R. P.; Facchetti, A.; Marks, T. J. *Chem. Rev.* **2010**, *110*, 205−239. (b) DiBenedetto, S.; Facchetti, A.; Ratner, M. A.; Marks, T. J. *Adv. Mater.* **2009**, *21*, 1407−1433.